Electroluminescence

Tuning Optical Properties by Controlled Aggregation: Electroluminescence Assisted by Thermally-Activated Delayed Fluorescence from Thin Films of Crystalline Chromophores

Ritesh Haldar,*[a] Marius Jakoby+,[b] Mariana Kozlowska+,[c] Motiur Rahman Khan+,[d] Hongye Chen,[a, e] Yohanes Pramudya,[c] Bryce S. Richards,[b, d] Lars Heinke,[a] Wolfgang Wenzel,[c] Fabrice Odobel,[f] Stéphane Diring,*[f] Ian A. Howard,[b, d] Uli Lemmer,[b, d] and Christof Wöll*[a]

Abstract: Several photophysical properties of chromophores depend crucially on intermolecular interactions. Thermally-activated delayed fluorescence (TADF) is often influenced by close packing of the chromophore assembly. In this context, the metal-organic framework (MOF) approach has several advantages: it can be used to steer aggregation such that the orientation within aggregated structures can be predicted using rational approaches. We demonstrate this design concept for a DPA-TPE (diphenylamine-tetraphenylethylene) chromophore, which is non-emissive in its solvated state due to vibrational quenching. Turning this DPA-TPE into a ditopic linker makes it possible to grow oriented MOF thin films exhibiting pronounced green electroluminescence with low onset voltages. Measurements at different temperatures clearly demonstrate the presence of TADF. Finally, this work reports that the layer-by-layer process used for MOF thin film deposition allows the integration of the TADF-DPA-TPE in a functioning LED device.

Organic light emitting molecules, explored for solid-state lighting (SSL) and display applications, face a number of challenges; such as unpredictable, often amorphous organization (aggregation) in the bulk state and unwanted quenching of the photoexcitation energy.[1] In order to compete with inorganic semiconductors, these and related problems (e.g. facile electron-hole (e-h) injection and their controlled recombination in mesoscale assemblies) must be considered.

Recently, an intriguing class of chromophores of pronounced interest for integration in OLEDs (organic light emitting diodes) has been introduced, namely organic compounds showing thermally activated delayed fluorescence (TADF).[2] In TADF emitters, light-emission efficiency is increased by populating singlet excited states (S) via a reverse intersystem crossing (RISC) from triplet state (T).[3] The RISC process allows converting a high fraction of the unwanted triplet excitons (T) generated by electrical excitation to singlet excitons to yield fluorescence and thus contribute to a high quantum efficiency. Previous works have demonstrated that TADF molecules can be integrated into working devices in its pristine state.[4] To avoid aggregation effects TADF molecules are also used by embedding in suitable host polymers.[2c]

[a] Dr. R. Haldar, H. Chen, Dr. L. Heinke, Prof. Dr. C. Wöll
Institute of Functional Interfaces (IFG)
Karlsruhe Institute of Technology (KIT)
Hermann-von-Helmholtz Platz-1, 76344, Eggenstein-Leopoldshafen (Germany)
E-mail: ritesh.haldar@kit.edu
christof.woell@kit.edu

[b] M. Jakoby,+ Prof. Dr. B. S. Richards, Dr. I. A. Howard, Prof. Dr. U. Lemmer
Institute of Microstructure Technology (IMT)
Karlsruhe Institute of Technology (KIT)
Hermann-von-Helmholtz Platz-1, 76344, Eggenstein-Leopoldshafen (Germany)

[c] Dr. M. Kozlowska,+ Dr. Y. Pramudya, Prof. Dr. W. Wenzel
Institute of Nanotechnology (INT)
Karlsruhe Institute of Technology (KIT)
Hermann-von-Helmholtz Platz-1, 76344, Eggenstein-Leopoldshafen (Germany)

[d] Dr. M. Rahman Khan,+ Prof. Dr. B. S. Richards, Dr. I. A. Howard, Prof. Dr. U. Lemmer
Light Technology Institute (LTI)
Karlsruhe Institute of Technology (KIT)
Engesserstrasse 13, 76131, Karlsruhe (Germany)

[e] H. Chen
State Key Laboratory of Mechanics and Control of Mechanical Structures
Key Laboratory for Intelligent Nano Materials and Devices of Ministry of Education
Institute of Nano Science, Nanjing (P. R. China)

[f] Prof. Dr. F. Odobel, Dr. S. Diring
CNRS, Chimie et Interdisciplinarité: Synthèse, Analyse, Modélisation
Université de Nantes
CEISAM, UMR 6230, 4400 Nantes (France)
E-mail: stephane.diring@univ-nantes.fr

[+] These authors contributed equally to this work.

Supporting information and the ORCID identification numbers for the authors of this article can be found under: https://doi.org/10.1002/chem.202003712.

The unwanted, aggregation-induced effects can be avoided by employing the metal–organic framework (MOF) approach.[5] MOFs as a thin film can be grown on functionalized substrates to chromophoric linkers are connected by metal or metal-oxo nodes, yielding crystalline solids with predictable and controllable structure. realize optically active, crystalline materials. In these MOFs, The rational assembly process is highly advantageous for designing dense arrays of optically active chromophores resulting in materials with excellent properties such as high quantum yield emission,[6] efficient energy transfer,[7] and/or excellent nonlinear optical responses.[8] Some of the most pertinent problems in connection with using chromophores showing TADF at high densities, that is, concentration quenching and solvent-induced effects,[6,9] can be avoided by our approach of integrating the TADF chromophore as a linker in a MOF thin film. In addition, the fact that the structure of resulting solids is predictable allows applying theoretical methods for a virtual screening of possible compounds prior to experimental realization.[9b]

Despite great promise as a light emitting material for SSL and display application,[10] the common form of MOFs, that is, powders, cannot be integrated into a device structure in a straightforward fashion. For this reason, a number of methods have been developed to provide monolithic MOF coatings.[11] One of the most versatile methods in this context is the layer-by-layer (lbl) liquid-phase epitaxy (LPE) method to realize oriented, monolithic, and transparent thin films of crystalline MOFs with high optical quality on a desired substrate with controllable thickness.[12] Such surface-anchored MOF thin films(SURMOFs) have already been used successfully for device fabrication.[13] Here, we demonstrate that SURMOFs are also well suited to realize bright emissive crystalline films based on TADF emitters and to integrate them in a working device.

In contrast to the common examples of TADF active chromophores, here we use a new chromophore, diphenylamine-tetraphenylethylene (DPA-TPE), showing aggregation-induced emission (synthesis scheme shown in the Supporting Information). DPA-TPE is non-emissive in the solvated state but exhibits its TADF when assembled in a crystalline MOF thin film (Figure 1 a–b). The role of crystalline aggregate like packing on the TADF efficiency is elucidated by a detailed photophysical analysis of the RISC mechanism (Figure 1 c). The TADF-active SURMOF was integrated as an emitting layer in a LED device, exhibiting an efficient green electroluminescence (EL) with a maximum luminance of 270 cd m^{-2} (Figure 1 b). A theoretical insight into the chromophore assembly and its excited state dynamics, followed by control experimental observations, revealed the role of the TADF process for the unprecedented EL efficiency from a MOF thin film. The key property of TADF-active chromophores is to facilitate the coupling of the excited triplet (T) state to the singlet (S) state. While the other direction, S→T conversion or intersystem crossing (ISC) is rather common, transfer of molecules from T to S states, the reverse intersystem crossing (RISC) requires suitable molecular architectures. A common approach to achieve RISC is to carefully combine electron donor and acceptor units within a chromophore, so as to allow for intramolecular charge transfer (ICT).

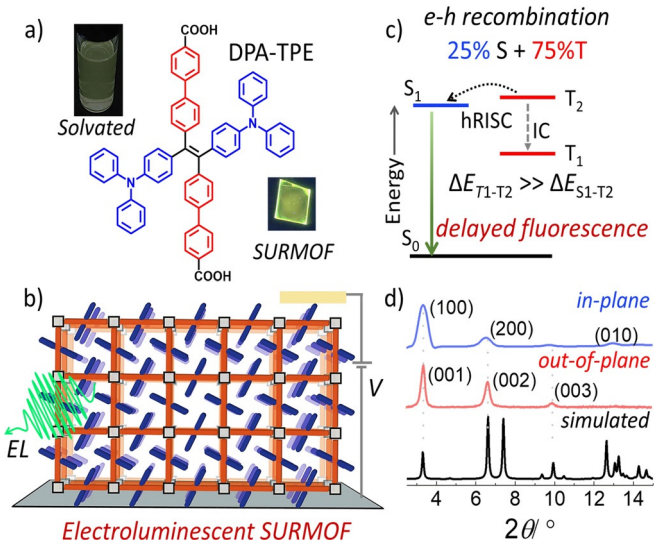

Figure 1. a) Chemical structure of DPA-TPE linker and its turn-on emissive feature in SURMOF state; b) electroluminescence (EL) in the DPA-TPE based SURMOF, enforced by coordination and periodic stacking; c) energy diagram of the singlet (S) and triplet (T) states of DPA-TPE in SURMOF, demonstrating "hot exciton" reverse intersystem crossing (hRISC) process; d) simulated and experimental out- and in-plane *x*-ray diffraction patterns of Zn-DPA-TPE (**1**).

Numerous design strategies have been reported, and in a number of cases efficient TADF has been shown to result from combining multiple separate photophysical processes, including charge transfer (CT) and locally excited states.[2c,14] In most TADF chromophores (i) the highest occupied molecular orbital (HOMO) is well separated from lowest unoccupied molecular orbital (LUMO), and (ii) the energy gap between the T and S excited states (ΔE_{ST}) amounts to less that ≈0.2 eV.[3] Key requirement for TADF is a sufficient RISC rate and a radiative decay rate of $\geq 10^6$ s^{-1} from the lowest singlet excited state (S_1).[3] Additionally, an efficient RISC requires a close to resonance condition of the localized and charge transfer T states.[15]

Currently investigated TADF chromophores involving CT excited state are highly sensitive to their environment and device fabrication requires embedding these photoactive moieties in a protecting, optically inactive polymer matrix. In our approach, we use a more controlled process by assembling the chromophores into a crystalline framework with a density only slightly lower than the corresponding molecular solid. The basis for the work shown here is a donor-acceptor-donor DPA-TPE (diphenylamine-tetraphenylethylene) chromophore. Two carboxylic acid groups were added to turn this emitter into a chromophoric MOF linker (Figure 1 a and Figure S1, Supporting Information).

In the solvated state, due to free rotation of phenyl groups in the TPE unit,[16] nonradiative decay of the excited state dominates and DPA-TPE is nonemissive (Figure 1 a and S2). When assembling the DPA-TPE linkers into the MOF, a crystalline-aggregate is formed. By this enforced packing, the rotational freedom of the phenyl groups is restricted, and the images shown in Figure 1 a reveal the pronounced difference of emission in the solvated and the crystalline aggregate (MOF) state (aggregation induced emission).

The precise arrangement of the DPA-TPE chromophores in the SURMOF-2[17] type structure realized here is shown in Figure 1b and S3a. A 2D square grid-like network is formed by Zn-paddlewheel secondary building units (SBUs) linked together with ditopic chromophoric linkers. These 2D sheets stacked along the crystallographic [010] direction, which in the SURMOF used here is oriented parallel to the substrate. Inspection of Figure S3a reveals that the linkers are rather closely packed. Details of the fabrication process of the SURMOFs from Zn-acetate and DPA-TPE ethanolic solutions -OH functionalized surfaces of quartz glass/SiO_2 are provided in the Supporting Information. The process yielded highly uniform, transparent MOF thin films of Zn-DPA-TPE (**1**) (Figure S3b). The out-of-plane and in-plane X-ray diffraction (XRD) data revealed the presence of a well-defined SURMOF-2 type structure,[17b] with unit cell dimensions of $a=b=2.6$ nm and $c=0.7$ nm (Figure 1d).

As pointed out above, the crystalline packing of DPA-TPE in **1** is rather dense. In analogy to previously reported SURMOF-2 type structure we thus expected strong inter-chromophore interactions.[7b,18] This expectation is confirmed by the UV/Vis data shown in Figure 2a recorded for **1** and the solvated (ethanol) DPA-TPE linkers. The DPA-TPE linker exhibited an absorption band at ≈3.26–2.76 eV, attributed to ICT from the DPA to the TPE unit (gray, Figure 2a). As pointed out above, this compound shows only weak fluorescence in the solvated state (Figure S2). Measurement of the fluorescence life-time revealed a value of ≈1.5 ns (gray, Figure 2b). Upon packing the chromophores in SURMOF, the broad ICT absorption band is shifted to slightly lower energies, ≈3.30–2.58 eV (Figure 2a). In pronounced contrast to the solvated state, now strong fluorescence is observed, with considerably longer life-time of ≈4 ns (excitation at 3.1 eV, Figure 2b and S4). To confirm the presence of the TADF process, a long-decay fluorescence measurement was carried out on **1** using an excitation energy of 3.1 eV. This yielded a substantially delayed fluorescence life-time of ≈200 μs (Figure 2c, green). We have compared the prompt vs. delayed fluorescence components of **1** with that of the solid (powder), amorphous DPA-TPE linker. This indicated that in **1** delayed fluorescence component is more dominant than in case of the powder state of DPA-TPE (Figure 2c, black). This once more demonstrates the beneficial effect of a highly ordered crystalline assembly for the TADF process.

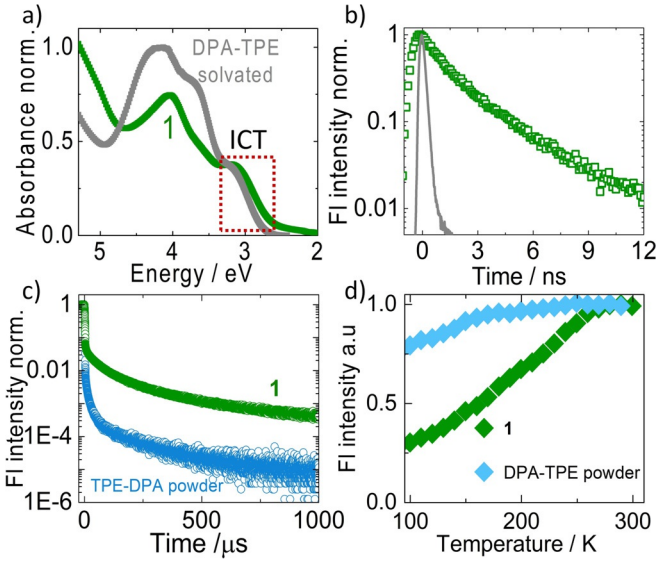

Figure 2. a) UV/Vis spectra of **1** and DPA-TPE (20 μM, ethanol), ICT = intramolecular charge transfer; b) prompt fluorescence decay (monitored at 2.29–2.13 eV) of **1** and DPA-TPE (20 μM, ethanol); c) delayed fluorescence in **1** and DPA-TPE powder; d) temperature dependent fluorescence intensity in **1** and DPA-TPE powder; (a.u. = arbitrary unit).

Since the delayed fluorescence is due to thermal excitation of T to S state, the temperature dependence of fluorescence was investigated. We observed that an increase in temperature from 100 to 300 K increased the emission intensity of **1** by a factor of ≈3.3, thus confirming that T states are thermally excited to S states (green, Figure 2d, Figure S4). Again, this effect is substantially different from the amorphous powder state of the DPA-TPE linker, where the enhancement amounts to only 1.25 (blue in Figure 2d). The fluorescence quantum yield (QY) of **1** was found to be rather high, 14 ± 2%.

After having demonstrated the turn-on TADF in **1**, we have explored the performance of these SURMOFs after integration in a LED device. To this end, a hole transporting layer (HTL; 30 nm *m*-MTDATA = 4,4′,4″-Tris[phenyl(*m*-tolyl)amino]triphenylamine) coated ITO was used as substrate for SURMOF deposition. An electron transporting layer (ETL; 30 nm TPBi = 2,2′,2″-(1,3,5-Benzinetriyl)-tris(1-phenyl-1-H-benzimidazole)) and cathode (LiF/Al) were deposited to on top of SURMOF layer to yield a LED device with ITO/HTL/**SURMOF**/ETL/LiF/Al configuration, as illustrated in the inset of Figure 3a.[19] We have deposited either the TADF-active **1** or a TADF-inactive **1** $\mathbf{c_{on}}$ (TPE linker-based SURMOF-2,[17b] TPE linker is identical in length with DPA-TPE, Figure S5, Fluorescence QY ≈34%) of ≈25–30 nm thickness directly, using the lbl process on the hole transporting layer coated ITO.

The LED device of **1** $\mathbf{c_{on}}$ indeed showed low luminance of 100 cd m^{-2} at 14 V, with a turn-on voltage of ≈6.4 V (Figure S5). Applying a higher bias 19 V lead to a moderate increase of luminance (130 cd m^{-2}). Replacing the TPE linker by the TADF-active linker, **1** lead to an improvement of performance (Figure 3a–b). A luminescence of 270 cd m^{-2} was observed already at 14 V, along with a ≈50 times larger current at 14 V and a lower turn-on voltage of 5.8 eV (@1 cd m^{-2}). These observations suggest that the improved electroluminescence observed in **1**, can be attributed to the improved charge transport and possibly to the presence of TADF process. Such electroluminescence at low voltages using a SURMOF or any other MOF thin film as active layer is comparable to the previous reports.[10c,d,f,20] The electroluminescence with high density TADF chromophores indicates that the SURMOF enables i) a high quality interface between SURMOF and transport layer, ii) reduced defects in SURMOF due its crystalline order allowing better charge transport and iii) efficient TADF process due to the controlled environment of individual chromophores.

The mechanism of the observed TADF was revealed by time-dependent density functional theory calculations (TD-DFT) of the DPA-TPE excited states in SURMOF-2 using *meta*-GGA-

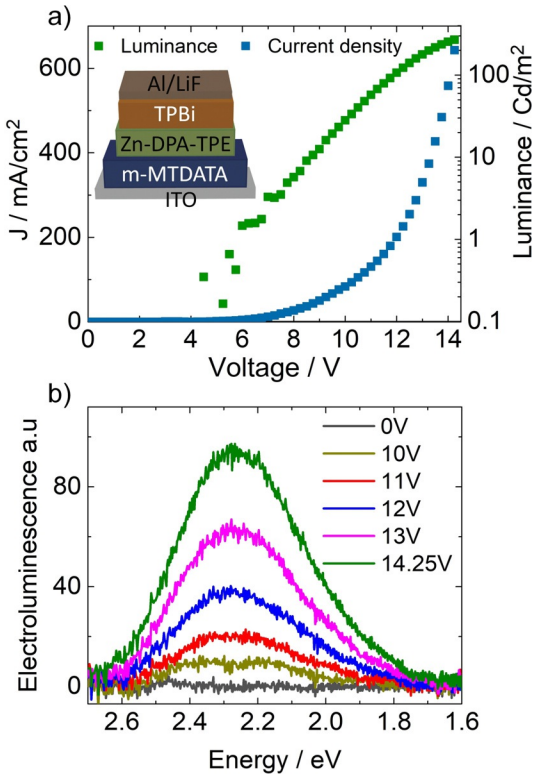

Figure 3. a) Current density and luminance of **1**, with different applied voltages, inset: LED device structure of **1**; b) Electroluminescence spectra of **1** obtained at different applied voltages, using a device configuration shown above; (a.u. = arbitrary unit).

hybrid BMK/def2-SVP + D3 in unrestricted formalism[21] and a quantum mechanics/molecular mechanics (QM/MM) approach[22] (see supporting information, Figure S6). The specific SURMOF-2 packing reduces the adiabatic energy gap ΔE_{ST} between S_1 and T_2 excited states from those for the free molecule of 0.354 to ≈0.24 eV. These results allow to unambiguously demonstrate the influence of MOF assemblies on the presence of "hot exciton" mechanism of TADF and the efficient conversion of triplets into singlets, which then provide efficient emission of photons.

The analysis of the theoretical results for the hole and electron densities of DPA-TPE (Figure 4) in S_1, T_1 and T_2 excited states proves their hybridized local and charge transfer (HLCT)[23] nature with the h-e overlap of 0.67, 0.84 and 0.81 a.u., respectively (Figure S7). Partial CT character of S_1 and T_2 is directly connected to the spatial separation of HOMO and LUMO orbitals of DPA-TPE in MOF (Figure 4, Figures S7 and S8), necessary for TADF.[24] Further, insight of the S_1, T_1 and T_2 excited state's geometries revealed the key reasons for an efficient spin-orbit coupling[25] between S_1 and T_2 states (see Figures S9 and S10).

Restriction of intramolecular motion of DPA-TPE in SURMOF-2 activates both, ISC and RISC between the high-lying triplet (T_2) and the lowest singlet state (S_1) with the rates of 6.94×10^6 s^{-1} and 1.91×10^7 s^{-1}, respectively (at 300 K, Figure S11), calculated by Fermi's golden rule using semi-classical Marcus theory[26] (see Supporting Information). According to the

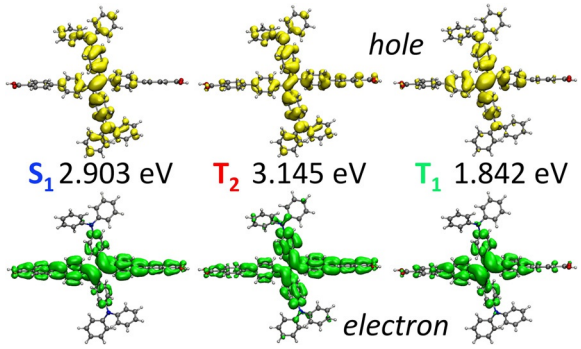

Figure 4. Visualization of hole (in yellow) and electron (in green) densities (isovalue of 0.0005 a.u.) upon excitation to S_1, T_1 and T_2 states, calculated using Multiwfn (version 3.6) analyzer, with listed adiabatic energies of the excited state with regard to the ground state.

energy-gap law,[27] splitting of energy levels of DPA-TPE in SURMOF-2 with large energy gap between T_2 and T_1 (1.3 eV) facilitates (i) the "hot exciton" RISC process from T_2 to S_1 and (ii) largely restricts the IC from T_2 to T_1 (Figure 1 c).

In conclusion, we have demonstrated the first example of an electroluminescent SURMOF based on chromophores showing TADF. The chromophoric linker, while nonemissive in the solvated state, exhibits pronounced prompt and delayed fluorescence after aggregation into the crystalline MOF lattice. A theoretical analysis revealed that the stacking-induced restrictions of the free molecule's torsional vibrations, resulting in the small reorganization energy and the lowering of the T-S energy gap within the MOF are the main reasons for the "turning on" of the DPA-TPE linkers. Furthermore, the high potential for the layer-by-layer process for integration of SURMOFs is demonstrated by fabricating an LED device with low turn-on voltage. In future work computational screening for example, using the SCU-approach[9b] approach is expected to lead to a pronounced increase in luminescence of SURMOF-LEDs.

Acknowledgements

This research has been funded by the Deutsche Forschungsgemeinschaft (DFG, German Research Foundation) under Germany Excellence Strategy via the Excellence Cluster 3D Matter Made to Order (Grant No. EXC-2082/1-390761711). The authors acknowledge the funding by the Virtual Materials Design (VirtMat) initiative at KIT. This work was performed on the computational resource ForHLR II funded by the Ministry of Science, Research and the Arts of Baden-Württemberg and the DFG. This work is also supported by ANR PhotoMOF project, Grant ANR-18-CE05-0008-01. M.K. is very grateful to M. Krstić for fruitful discussions and code developments. H.C. acknowledges financial support from China Scholarship Council. The authors acknowledge J. Hémez and L. Arzel for mass spectrometry analysis at the AMaCC platform (CEISAM UMR CNRS 6230, University of Nantes). Open access funding enabled and organized by Projekt DEAL.

Conflict of interest

The authors declare no conflict of interest.

Keywords: aggregation · electroluminescence · epitaxial thin film · metal–organic frameworks · thermally activated delayed fluorescence

[1] A. P. Green, A. R. Buckley, *Phys. Chem. Chem. Phys.* **2015**, *17*, 1435 – 1440.
[2] a) X.-K. Chen, D. Kim, J.-L. Brédas, *Acc. Chem. Res.* **2018**, *51*, 2215 – 2224; b) A. Endo, K. Sato, K. Yoshimura, T. Kai, A. Kawada, H. Miyazaki, C. Adachi, *Appl. Phys. Lett.* **2011**, *98*, 083302; c) Z. Yang, Z. Mao, Z. Xie, Y. Zhang, S. Liu, J. Zhao, J. Xu, Z. Chi, M. P. Aldred, *Chem. Soc. Rev.* **2017**, *46*, 915 – 1016.
[3] H. Uoyama, K. Goushi, K. Shizu, H. Nomura, C. Adachi, *Nature* **2012**, *492*, 234 – 238.
[4] a) X. Cai, Z. Qiao, M. Li, X. Wu, Y. He, X. Jiang, Y. Cao, S.-J. Su, *Angew. Chem. Int. Ed.* **2019**, *58*, 13522 – 13531; *Angew. Chem.* **2019**, *131*, 13656 – 13665; b) L. Derue, S. Olivier, D. Tondelier, T. Maindron, B. Geffroy, E. Ishow, *ACS Appl. Mater. Interfaces* **2016**, *8*, 16207 – 16217.
[5] R. Haldar, L. Heinke, C. Wöll, *Adv. Mater.* **2020**, *32*, 1905227.
[6] Z. Wei, Z.-Y. Gu, R. K. Arvapally, Y.-P. Chen, R. N. McDougald, J. F. Ivy, A. A. Yakovenko, D. Feng, M. A. Omary, H.-C. Zhou, *J. Am. Chem. Soc.* **2014**, *136*, 8269 – 8276.
[7] a) J. Jia, L. Gutiérrez-Arzaluz, O. Shekhah, N. Alsadun, J. Czaban-Jozwiak, S. Zhou, O. M. Bakr, O. F. Mohammed, M. Eddaoudi, *J. Am. Chem. Soc.* **2020**, *142*, 8580 – 8584; b) R. Haldar, M. Jakoby, A. Mazel, Q. Zhang, A. Welle, T. Mohamed, P. Krolla, W. Wenzel, S. Diring, F. Odobel, B. S. Richards, I. A. Howard, C. Wöll, *Nat. Commun.* **2018**, *9*, 4332; c) Q. Zhang, C. Zhang, L. Cao, Z. Wang, B. An, Z. Lin, R. Huang, Z. Zhang, C. Wang, W. Lin, *J. Am. Chem. Soc.* **2016**, *138*, 5308 – 5315.
[8] a) R. Medishetty, J. K. Zaręba, D. Mayer, M. Samoć, R. A. Fischer, *Chem. Soc. Rev.* **2017**, *46*, 4976 – 5004; b) L. R. Mingabudinova, V. V. Vinogradov, V. A. Milichko, E. Hey-Hawkins, A. V. Vinogradov, *Chem. Soc. Rev.* **2016**, *45*, 5408 – 5431; c) M. Oldenburg, A. Turshatov, D. Busko, S. Wollgarten, M. Adams, N. Baroni, A. Welle, E. Redel, C. Wöll, B. S. Richards, I. A. Howard, *Adv. Mater.* **2016**, *28*, 8477 – 8482.
[9] a) J. Yu, Y. Cui, H. Xu, Y. Yang, Z. Wang, B. Chen, G. Qian, *Nat. Commun.* **2013**, *4*, 2719; b) R. Haldar, A. Mazel, M. Krstić, Q. Zhang, M. Jakoby, I. A. Howard, B. S. Richards, N. Jung, D. Jacquemin, S. Diring, W. Wenzel, F. Odobel, C. Wöll, *Nat. Commun.* **2019**, *10*, 2048.
[10] a) H. Mieno, R. Kabe, N. Notsuka, M. D. Allendorf, C. Adachi, *Adv. Opt. Mater.* **2016**, *4*, 1015 – 1021; b) H. Mieno, R. Kabe, M. D. Allendorf, C. Adachi, *Chem. Commun.* **2018**, *54*, 631 – 634; c) M. Gutiérrez, C. Martin, K. Kennes, J. Hofkens, M. Van der Auweraer, F. Sánchez, A. Douhal, *Adv. Opt. Mater.* **2018**, *6*, 1701060; d) G. Haider, M. Usman, T.-P. Chen, P. Perumal, K.-L. Lu, Y.-F. Chen, *ACS Nano* **2016**, *10*, 8366 – 8375; e) Q. Gong, Z. Hu, B. J. Deibert, T. J. Emge, S. J. Teat, D. Banerjee, B. Mussman, N. D. Rudd, J. Li, *J. Am. Chem. Soc.* **2014**, *136*, 16724 – 16727; f) D. Chen, H. Xing, Z. Su, C. Wang, *Chem. Commun.* **2016**, *52*, 2019 – 2022; g) J. Li, S. Yuan, J.-s. Qin, L. Huang, R. Bose, J. Pang, P. Zhang, Z. Xiao, K. Tan, A. V. Malko, T. Cagin, H.-C. Zhou, *ACS Appl. Mater. Interfaces* **2020**, *12*, 26727 – 26732.
[11] a) I. Stassen, M. Styles, G. Grenci, H. V. Gorp, W. Vanderlinden, S. De Feyter, P. Falcaro, D. D. Vos, P. Vereecken, R. Ameloot, *Nat. Mater.* **2016**, *15*, 304 – 310; b) E. Virmani, J. M. Rotter, A. Mähringer, T. von Zons, A. Godt, T. Bein, S. Wuttke, D. D. Medina, *J. Am. Chem. Soc.* **2018**, *140*, 4812 – 4819.
[12] J. Liu, C. Wöll, *Chem. Soc. Rev.* **2017**, *46*, 5730 – 5770.
[13] a) V. Stavila, A. A. Talin, M. D. Allendorf, *Chem. Soc. Rev.* **2014**, *43*, 5994 – 6010; b) L. Heinke, C. Wöll, *Adv. Mater.* **2019**, *31*, 1806324.
[14] K. Li, Y. Zhu, B. Yao, Y. Chen, H. Deng, Q. Zhang, H. Zhan, Z. Xie, Y. Cheng, *Chem. Commun.* **2020**, *56*, 5957 – 5960.
[15] a) R. S. Nobuyasu, Z. Ren, G. C. Griffiths, A. S. Batsanov, P. Data, S. Yan, A. P. Monkman, M. R. Bryce, F. B. Dias, *Adv. Opt. Mater.* **2016**, *4*, 597 – 607; b) M. K. Etherington, J. Gibson, H. F. Higginbotham, T. J. Penfold, A. P. Monkman, *Nat. Commun.* **2016**, *7*, 13680.
[16] N. B. Shustova, B. D. McCarthy, M. Dincă, *J. Am. Chem. Soc.* **2011**, *133*, 20126 – 20129.
[17] a) J. Liu, B. Lukose, O. Shekhah, H. K. Arslan, P. Weidler, H. Gliemann, S. Bräse, S. Grosjean, A. Godt, X. Feng, K. Müllen, I.-B. Magdau, T. Heine, C. Wöll, *Sci. Rep.* **2012**, *2*, 921; b) R. Haldar, S. Diring, P. K. Samanta, M. Muth, W. Clancy, A. Mazel, S. Schlabach, F. Kirschhöfer, G. Brenner-Weiß, S. K. Pati, F. Odobel, C. Wöll, *Angew. Chem. Int. Ed.* **2018**, *57*, 13662 – 13665; *Angew. Chem.* **2018**, *130*, 13850 – 13854.
[18] a) R. Haldar, A. Mazel, R. Joseph, M. Adams, I. A. Howard, B. S. Richards, M. Tsotsalas, E. Redel, S. Diring, F. Odobel, C. Wöll, *Chem. Eur. J.* **2017**, *23*, 14316 – 14322; b) R. Haldar, K. Batra, S. M. Marschner, A. B. Kuc, S. Zahn, R. A. Fischer, S. Bräse, T. Heine, C. Wöll, *Chem. Eur. J.* **2019**, *25*, 7847 – 7851.
[19] C. Y. K. Chan, J. W. Y. Lam, Z. Zhao, S. Chen, P. Lu, H. H. Y. Sung, H. S. Kwok, Y. Ma, I. D. Williams, B. Z. Tang, *J. Mater. Chem. C* **2014**, *2*, 4320 – 4327.
[20] a) Z. You, H. Li, L. Zhang, B. Yu, J. Zhang, X. Wu, *J. Phys. Chem. C* **2017**, *121*, 23072 – 23079; b) R. Ballesteros-Garrido, A. P. da Costa, P. Atienzar, M. Alvaro, C. Baleizão, H. García, *RSC Adv.* **2016**, *6*, 35191 – 35196.
[21] a) A. D. Boese, J. M. L. Martin, *J. Chem. Phys.* **2004**, *121*, 3405 – 3416; b) F. Weigend, R. Ahlrichs, *Phys. Chem. Chem. Phys.* **2005**, *7*, 3297 – 3305; c) S. Grimme, J. Antony, S. Ehrlich, H. Krieg, *J. Chem. Phys.* **2010**, *132*, 154104.
[22] L. W. Chung, W. M. C. Sameera, R. Ramozzi, A. J. Page, M. Hatanaka, G. P. Petrova, T. V. Harris, X. Li, Z. Ke, F. Liu, H.-B. Li, L. Ding, K. Morokuma, *Chem. Rev.* **2015**, *115*, 5678 – 5796.
[23] a) Y. Xu, X. Liang, X. Zhou, P. Yuan, J. Zhou, C. Wang, B. Li, D. Hu, X. Qiao, X. Jiang, L. Liu, S.-J. Su, D. Ma, Y. Ma, *Adv. Mater.* **2019**, *31*, 1807388; b) W.-C. Chen, C.-S. Lee, Q.-X. Tong, *J. Mater. Chem. C* **2015**, *3*, 10957 – 10963.
[24] a) P. K. Samanta, D. Kim, V. Coropceanu, J.-L. Brédas, *J. Am. Chem. Soc.* **2017**, *139*, 4042 – 4051; b) Y. Olivier, J. C. Sancho-Garcia, L. Muccioli, G. D'Avino, D. Beljonne, *J. Phys. Chem. Lett.* **2018**, *9*, 6149 – 6163.
[25] X. Gao, S. Bai, D. Fazzi, T. Niehaus, M. Barbatti, W. Thiel, *J. Chem. Theory Comput.* **2017**, *13*, 515 – 524.
[26] R. Marcus, *J. Phys. Chem.* **1963**, *67*, 2889 – 2889.
[27] W. Li, Y. Pan, R. Xiao, Q. Peng, S. Zhang, D. Ma, F. Li, F. Shen, Y. Wang, B. Yang, Y. Ma, *Adv. Funct. Mater.* **2014**, *24*, 1609 – 1614.

Manuscript received: August 10, 2020
Revised manuscript received: September 6, 2020
Accepted manuscript online: September 7, 2020
Version of record online: November 17, 2020